Time-Domain Analysis of Graphene-based Miniaturized Antennas for Ultra-short-range Impulse Radio Communications

Sergi Abadal, Ignacio Llatser, Albert Mestres, Heekwan Lee, Eduard Alarcón, and Albert Cabellos-Aparicio

***Abstract*—Graphene is enabling a plethora of applications in a wide range of fields due to its unique electrical, mechanical, and optical properties. Among them, graphene-based plasmonic miniaturized antennas (or shortly named, *graphennas*) are garnering growing interest in the field of communications. In light of their reduced size, in the micrometric range, and an expected radiation frequency of a few terahertz, graphennas offer means for the implementation of ultra-short-range wireless communications. Motivated by their high radiation frequency and potentially wideband nature, this paper presents a methodology for the time-domain characterization and evaluation of graphennas. The proposed framework is highly vertical, as it aims to build a bridge between technological aspects, antenna design, and communications. Using this approach, qualitative and quantitative analyses of a particular case of graphenna are carried out as a function of two critical design parameters, namely, chemical potential and carrier mobility. The results are then compared to the performance of equivalent metallic antennas. Finally, the suitability of graphennas for ultra-short-range communications is briefly discussed.**

***Index Terms*—Graphene-based Antennas, Graphennas, Plasmonics, Time Domain Analysis, Terahertz, Emerging, Ultra-short-range Communications, Impulse Radio**

I. Introduction

NANOTECHNOLOGY is enabling the development and manufacture of systems with nanometric precision, leading not only to a further miniaturization of existing systems, but also to the creation of new systems that take advantage of the unique characteristics of nanomaterials [1]. Within this context, novel applications may require smaller forms of wireless communication while maintaining certain application-dependent performance in terms of bandwidth, transmission range or energy consumption.

Wireless Networks-on-Chip (WNoCs) [2] and Wireless NanoSensor Networks (WNSNs) [3], [4] constitute two clear examples of nanotechnology-enabled applications that would greatly benefit from ultra-short-range wireless communications. On the one hand, the WNoC paradigm consists in using on-chip antennas to wirelessly communicate components integrated within a chip, thereby addressing several performance challenges of current interconnects. On the other hand, WNSNs aim to enable wireless communication among nanosensors, seeking to exploit their novel sensing capabilities in locations not reachable with conventional sensors or in scenarios requiring a very high accuracy or deployment density.

In both cases, evident area constraints impose the use of antennas a few micrometers in size. Scaling metallic antennas down to such dimensions is not a practical approach, since the low conductivity of nanoscale metallic structures [5] leads to a poor antenna performance. Moreover, metallic antennas of a few micrometers have a resonant frequency of several hundreds of terahertz. Such frequency band is not suitable for RF wireless communications due both to its huge channel attenuation leading to an extremely limited communication range and to the difficulty of implementing transceivers operating at such high frequency band.

Alternatively, graphene-based plasmonic antennas, or shortly named *graphennas*, are uniquely suited for wireless communication within this context [6], [7]. By virtue of its plasmonic properties, a graphenna several micrometers long is able to radiate within the terahertz band (0.1 - 10 THz) [8], this is, two orders of magnitude lower than that of metallic antennas. Low-complexity and low-power solutions for the transceivers operating at such frequencies could be achieved by adopting impulse-based modulations [9], [10]. Furthermore, graphennas are tunable [11], [12] and show a higher radiation efficiency than typical THz metallic antennas despite their size difference [13], [14].

Graphennas have recently attracted substantial research efforts. Several works have focused on modeling the subwavelength plasmonic effects that allow them to radiate at lower frequencies than their metallic counterparts [8], [11], [15]–[21], whereas other investigations have resulted in the proposal of various graphenna configurations [12], [22]–[25]. However, the behavior of graphene antennas has not been examined in the time domain yet. Broadband antennas in general, and those oriented to impulse radio in particular, are generally characterized by means of time-domain techniques as the number of frequency points that must be measured becomes extremely large in order to obtain accurate results. Hence, in light of not only the potentially wideband nature of the

This work was supported by Samsung under the Global Research Outreach (GRO) Program, INTEL under the Doctoral Student Honor Program, and by the Technical University of Catalunya (UPC). This work has been also partially supported by the FI-AGAUR grant of the Catalan Government and the FPU grant of the Spanish Ministry of Education.

Sergi Abadal, Albert Mestres, Eduard Alarcón and Albert Cabellos Aparicio are with the NaNoNetworking Center in Catalonia (N3Cat) at Technical University of Catalunya, Barcelona, Spain. Corresponding Email: abadal@ac.upc.edu

Ignacio Llatser was with the NaNoNetworking Center in Catalonia (N3Cat) at Technical University of Catalunya, Barcelona, Spain. He is now with the Vodafone Chair for Mobile Communication Systems, Technical University of Dresden, 01062 Dresden, Germany.

Heekwan Lee is with the Samsung Advanced Institute of Technology (SAIT), Suwon 440-600, Korea.

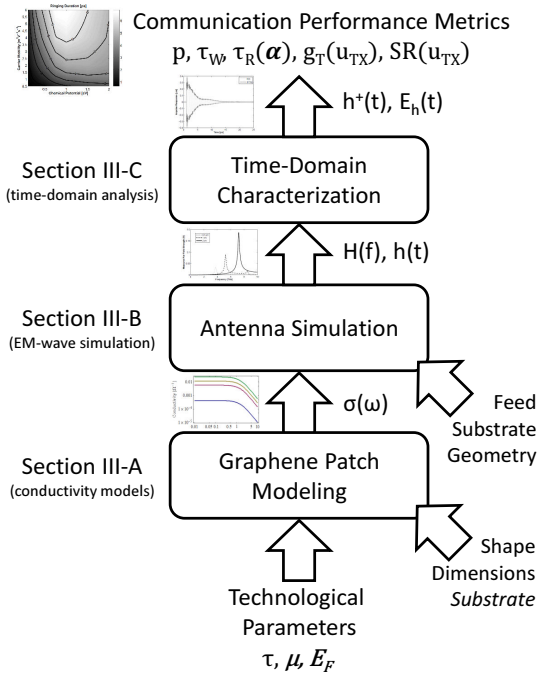

Fig. 1. Main contribution of this work: a methodology that allows assessing the communication performance of graphene-based antennas in the time domain as a function of the technological parameters of graphene. To this end, the framework combines conductivity models and electromagnetic simulation with time-domain characterization.

graphennas, but also their very high radiation frequency, it is reasonable to think that their response will be measured in the time domain whenever this possibility is feasible.

As the main contribution, this work proposes a general methodology for the evaluation of the communication performance of graphene-based antennas in the time domain. We use a vertical approach, summarized in Fig. 1, in an attempt to bridge the conceptual gap between the technological parameters of graphene and the communication performance of graphennas. This is a necessary step towards understanding the variations in terms of communication performance that occur when these parameters are modified, in the pathway to obtaining models that faithfully describe the relation between both ends. We expect that the proposed framework will also allow designers to set minimum graphene quality or chemical potential requirements based on application-dependent communication performance guidelines. Related works have inspected the impact of key technological parameters upon the antenna performance [11], [17], [19], but not from a communications standpoint. Even though other works have inspected the impact of graphene parameters upon the communication performance of graphene-based photodetectors [26] or Förster Resonance Energy Transfer schemes [27], this is, to the best of the authors knowledge, the first work that discusses such possibility for the time-domain characterization of graphennas.

The proposed methodology is employed in this paper to assess the suitability of graphennas for ultra-short-range impulse radio communications. We first analyze the impact of two key parameters of graphene, i.e. chemical potential and carrier mobility, upon the temporal response of a particular graphenna design. Its performance is then compared with that of a same-size metallic antenna and of metallic antenna with the same radiation frequency. Finally, we propose a figure of merit that jointly evaluates antennas in terms of radiation efficiency and transmitted pulse dispersion. This figure of merit could be used for the optimization of the communication performance by means of a transceiver-graphenna co-design process.

The remainder of the is as follows. In Section II, we briefly summarize the fundamentals of graphene-based plasmonic miniaturized antennas and review recent investigations based on these novel antennas. The concepts and definitions contained therein will be used in Section III, where we detail the methodology proposed as the main contribution of this work and particularize it to a given graphenna design. In Section IV, we present the results of the time-domain characterization and suggest a new figure of merit. Finally, Section V concludes the paper.

II. Graphene-based Plasmonic Miniaturized Antennas

Graphene, a flat monolayer of carbon atoms tightly packed in a two-dimensional honeycomb lattice, has recently attracted the attention of the research community due to its extraordinary mechanical, electronic, and optical properties [28]. Graphene allows to utilize novel physics in a plethora of potential applications, ranging from ultra-high-speed transistors [29] to transparent solar cells [30], meta-materials [31] and graphene plasmonics [32]–[34]. In particular, the application of carbon materials in the realm of antennas was first discussed in [35]–[37]. Carbon nanotubes were proposed as potential dipole antennas and their transmission line properties and radiation pattern were analyzed. Still, the employment of carbon nanotubes involves several drawbacks in terms of manufacturing, tuning, and placement on planar implementation processes.

Alternatively, the possibility of employing micrometric graphene patches for wireless communication was first investigated in [8]. Following the work by Hanson on the propagation of electromagnetic waves on laterally-infinite graphene layers [38], it was demonstrated that a graphene patch a few micrometers long and wide would resonate in the terahertz band [8], [15], [16]. This directly contrasts with the behavior of metallic antennas, which have a resonant frequency up to two orders of magnitude higher for the same antenna size [39], [40].

Such discovery has lead to the surge of graphene antenna proposals that, in essence, consist of a number of finite-size graphene layers (the radiating elements) mounted over a metallic flat surface (the ground plane), with a dielectric material in-between and a feed to drive the signals to the antenna. Patch antenna configurations have been analyzed with a pin feed [11], a punctual excitation [23] or a graphene microstrip line at one edge of the graphene layer [24], [41]. Dipole-like designs, where the source is placed in the middle of two identical graphene layers, has been also proposed in [12], [22], [42]. Different biasing schemes have been also included in most of these works to take advantage of the unique tuning capabilities of graphennas [19], [23], [42]. Some of these proposals are conceptually represented in Fig. 2.

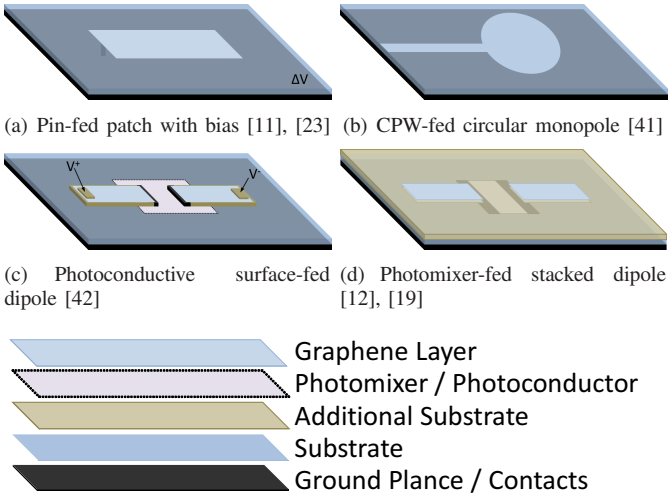

(a) Pin-fed patch with bias [11], [23] (b) CPW-fed circular monopole [41]

(c) Photoconductive surface-fed dipole [42] (d) Photomixer-fed stacked dipole [12], [19]

Fig. 2. Schematic representation of a set of graphene-based antennas proposed in the literature (see references [11], [12], [19], [23], [41], [42] for more details). Silicon lenses are used in (c) and (d) but not shown for simplicity.

The reason behind the subwavelength behavior of graphennas is the presence of *surface plasmon polariton* (SPP) waves on the surface of graphene. Such phenomenon occurs at the interface between any metallic and dielectric material pair when an electromagnetic wave impacts upon the metal. The properties of the SPP waves are determined by the frequency characteristics of the electrical conductivity of the metallic material (graphene in this case). For instance, while graphene shows strong plasmonic effects leading to resonance for frequencies in the terahertz band, other materials such as gold present this phenomenon in the optical range, hampering its employment for wireless communication purposes.

A. Conductivity Models

Recent studies related to the conductivity of graphene sheets [21] are enabling a precise modeling of the plasmonic phenomena occurring at the surface of graphennas [15]. The main approach considers that a graphenna of a few micrometers in size is large enough to disregard the effects of the graphene edges. Therefore, the model for infinite graphene sheets can be employed, in which case the conductivity is calculated by means of the Kubo formula [38]. Moreover, experimental results show that the Drude-like intraband contribution dominates in our frequency band of interest (0.1 - 10 THz), so that the conductivity can be expressed as:

$$\sigma(\omega) = \frac{2e^2}{\pi\hbar}\frac{k_B T}{\hbar}\ln\left[2\cosh\left[\frac{E_F}{2k_B T}\right]\right]\frac{i}{\omega + i\tau^{-1}}, \qquad (1)$$

where e, $\hbar$, and k_B are constants corresponding to the charge of an electron, the reduced Planck constant, and the Boltzmann constant, respectively [16], [17], [38]. Variables T, τ, and E_F correspond to the temperature, the relaxation time, and the chemical potential of the graphene layer. At mid-infrared and optical frequencies, the intraband contribution fades and the conductivity approaches a much lower universal value of $\sigma_0 = \pi e^2/(2h)$ [32].

The conductivity plays a major role in determining the resonance of the graphenna, since the wavelength of SPPs within the graphenna is λ/n_{eff}, where the effective mode index n_{eff} is dependent upon the conductivity as:

$$n_{eff}(\omega) = \sqrt{1 - 4\frac{\mu_0}{\epsilon_0}\frac{1}{\sigma(\omega)^2}}. \qquad (2)$$

Knowledge on the conductivity of graphene has led to a further investigation of the characteristics of graphennas. The surface impedance of graphennas has been investigated in [13], [43], allowing the extraction of preliminary results regarding the total efficiency of the graphenna. The impact of different substrates and their thickness upon the radiation characteristics of graphennas has been also studied in [17]. More importantly, the implications of varying the chemical potential and relaxation time of a graphenna were explored in [11] and are shown below.

B. Technological Design Parameters of Graphennas

Together with the antenna shape and dimensions, the conductivity plays a fundamental role in determining the radiation characteristics of the graphenna. As it is clearly observed in (1) and discussed next, the graphene conductivity strongly depends on the chemical potential and the relaxation time.

Chemical Potential - Also referred to as Fermi energy, the chemical potential E_F refers to the level in the distribution of electron energies at which a quantum state is equally likely to be occupied or empty. Since it is possible to control its value by applying an electrostatic bias or by means of chemical doping, the chemical potential can be considered as a design parameter for graphennas. The impact of the chemical potential upon the frequency response of the graphenna investigated in this work (see Fig. 5) is as shown in Fig. 3a, in accordance with the tendencies revealed in [11], [19]. It is observed that the radiation efficiency substantially increases with the chemical potential, whereas the resonant frequency is shifted upwards yet without an apparent effect on the resonance bandwidth. This confers graphennas unprecedented tuning possibilities that have been recently analyzed in different graphenna structures mostly at the terahertz band [12], [19], [22], [23], but also at microwave frequencies [20]; as well as in hybrid graphene-metallic antennas [25].

Relaxation Time - The relaxation time is the interval required for a material to restore a uniform charge density after a charge distortion is introduced and, in some works, it is expressed in terms of scattering rate Γ as $\Gamma = (2\tau)^{-1}$. At the band of interest (<10 THz), the relaxation time can be calculated as $\tau \approx \tau_{DC} = \mu\hbar\sqrt{n\pi}/(ev_F)$ [32], where μ is the carrier mobility, n is the carrier density, and v_F is the Fermi velocity. This implies neglecting phenomena such as interband damping or electron-phonon interaction, which appear over the interband and optical phonon threshold frequencies (∼50 THz) and cause the relaxation time to be dependent on a set of additional parameters. The carrier density relates to the chemical potential as $E_F = \sqrt{(\hbar v_F)^2 n\pi - (\pi K_B T)^2/3}$ [44]. On the contrary, the Fermi velocity does not depend on the Fermi energy and takes a value of $v_F = 3ta/(2\hbar) \approx 10^6$, where

$t \approx 2.8eV$ and $a = 1.42$Å are tight-binding parameters for graphene [45], [46]. Considering that $E_F \gg K_B T = 26\,meV$, the relaxation time is approximated as:

$$\tau \approx \mu \frac{E_F}{v_p^2}. \tag{3}$$

Fig. 3b shows the impact of the relaxation time upon the frequency response of the graphenna configuration investigated in this work (see Fig. 5). A stronger resonant behavior is observed as the relaxation time is increased, which matches the results in [11].

Carrier Mobility - The carrier mobility defines the average speed at which electrons can move within the material. Since diverse carrier mobility values can be achieved by means of different graphene manufacturing processes or by using different substrates [47], [48], we will consider it as a design parameter for graphennas. For a suspended layer of graphene, the carrier mobility is obtained as:

$$\mu = \frac{1}{ne\rho_{xx}}, \tag{4}$$

where $\rho_{xx}$is the sheet resistivity.

It is worth noting that (3) gives a direct relation between the carrier mobility and the relaxation time at the frequency band of interest. This implies that both parameters can be used interchangeably under the conditions assumed in this work and that, according to the results in Fig. 3b, a higher carrier mobility leads to a more resonant behavior.

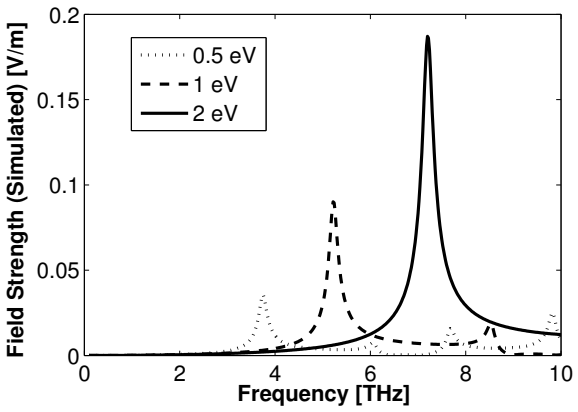

(a) $\tau = 1\,ps$, $E_F = \{0.5, 1, 2\}\,eV$

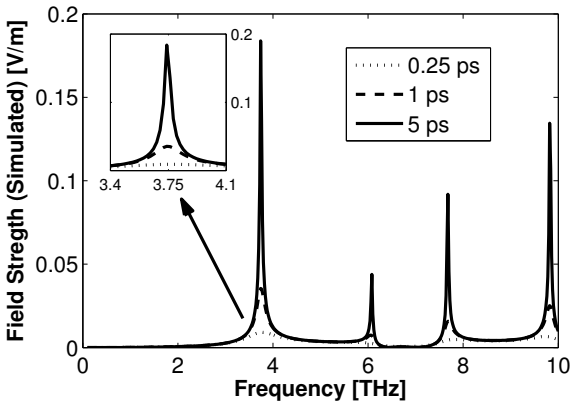

(b) $E_F = 0.5\,eV$, $\tau = \{0.25, 1, 5\}\,ps$

Fig. 3. Electric field strength at r = 1m of the investigated graphenna (see Fig. 5) as a function of frequency for different chemical potential and relaxation time values. The voltage inside the antenna is 1V for all frequencies. We refer the reader to Section III for further methodological details.

III. A Methodology for the Time-Domain Analysis of Graphennas

In this section, we detail the methodology proposed as the main contribution of this work. We also discuss the assumptions made when particularizing the framework to our case study (see Fig. 5 for details). Before that, though, we must define the concept of *impulse response* as it is the core of the characterization methodology. This need arises from the subtle discrepancies that different works have introduced in its specification [49]–[51]. We will mainly follow the notation and considerations employed in [51], which stem from the work in [50] and are summarized in Fig. 4.

Consider a time-dependent voltage $u_{TX}(t)$ delivered at the terminals of an antenna through a feed of characteristic impedance Z_{TX}. The radiated signal $e_{TX}(t, \theta, \phi)$ at the direction determined by the pair of angles $\{\theta, \phi\}$ is given by:

$$\frac{e_{TX}(t,\theta,\phi)}{\sqrt{Z_0}} = \frac{\delta(t - r/c_0)}{2\pi r c_0} * h_{TX}(t,\theta,\phi) * \frac{\partial}{\partial t}\frac{u_{TX}(t)}{\sqrt{Z_{TX}}}, \tag{5}$$

where the operator $*$ represents convolution, $h_{TX}(t, \theta, \phi)$ is the impulse response at the propagation direction, $\partial u_{TX}(t)/\partial t$ is the derivative of the input signal, r is the distance to the antenna, c_0 is the speed of light in vacuum, and Z_0 is the free space impedance [51]. From this equation, we infer that *the impulse response of an antenna is the relation between the excitation voltage of the antenna (input) and the radiated field strength (output)*. Therefore, the impulse response of any antenna can be obtained by applying a voltage to it and measuring, either physically or by means of simulation, the strength of the radiated fields. Note that this definition leaves the time derivative out of the impulse response of the antenna, as opposed to in [49], thus decoupling the differentiation effects inherent to all antennas from the antenna-dependent dispersion, impedance mismatch, and other losses. In the frequency domain, (5) becomes:

$$\frac{E_{TX}(f,\theta,\phi)}{\sqrt{Z_0}} = \frac{e^{j\omega r/c_0}}{2\pi r c_0} H_{TX}(f,\theta,\phi) j\omega \frac{U_{TX}(f)}{\sqrt{Z_{TX}}}, \tag{6}$$

where $E_{TX}(f, \theta, \phi)$ $H_{TX}(f, \theta, \phi)$, and U_{TX} are the radiated field, the response of the antenna, and the input voltage in the frequency domain. The delay is modeled with the exponential factor, whereas $j\omega$ is the equivalent to a time derivative.

A similar expression is used to calculate the voltage $u_{RX}(t)$ at the terminals of an antenna when receiving an electromagnetic $e_{RX}(t, \theta', \phi')$ wave arriving from the direction determined by the pair of angles $\{\theta', \phi'\}$:

$$\frac{u_{RX}(t)}{\sqrt{Z_{RX}}} = h_{RX}(t,\theta',\phi') * \frac{e_{RX}(t,\theta',\phi')}{\sqrt{Z_0}}, \tag{7}$$

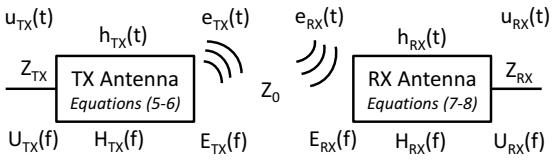

Fig. 4. Notation for a transmission and reception in the time domain (above) and in the frequency domain (below).

where $h_{TX}(t, \theta', \phi')$ is the impulse response of the receiving antenna at the incident direction and Z_{RX} is the characteristic impedance at the receiving end. With the definition of impulse response given in (5) and (7), the reciprocity theorem yields $h_{TX} = h_{RX}$ for the same antenna [51]. Note that this also applies in the case of graphene-based antennas, since the same plasmonic principles explain their operation both in transmission and in reception [15]. In the frequency domain, we have:

$$\frac{U_{RX}(f)}{\sqrt{Z_{RX}}} = H_{RX}(f, \theta', \phi') \frac{E_{RX}(f, \theta', \phi')}{\sqrt{Z_0}}, \tag{8}$$

with $U_{RX}(f)$, $H_{RX}(f, \theta', \phi')$, and $E_{RX}(f, \theta', \phi')$ as the frequency-domain versions of the voltage at the output, the antenna response, and the incident field. The reciprocity condition is still $H_{TX} = H_{RX}$ [51].

The main objective of the proposed methodology is to provide a way to characterize the behavior of graphennas in the time domain through its impulse response $h(t)$ (without loss of generality, the angles will hereafter be omitted from the notation). To this end, we first need to obtain $h(t)$ and then use time-domain metrics to characterize the performance of the antenna. The methodology is as summarized in Fig. 1:

1) The conductivity $\sigma(\omega)$ of a graphene layer with chemical potential E_F, relaxation time τ, and carrier mobility μ is modeled as explained in Section III-A.
2) The model of a graphene layer is integrated with the rest of antenna elements within an electromagnetic field solver, which allows to obtain the impulse response $h(t)$ by using (5)-(8) as indicated in Section III-B.
3) Finally, the communication performance of the whole graphenna is evaluated through a set of pre-defined metrics that require the impulse response $h(t)$ and a voltage waveform $u_{TX}(t)$ as inputs. These are detailed in Section III-C.

It is important to emphasize that, following these steps, we are able to express the different performance metrics as a function of the technological parameters of graphene.

A. Modeling the Graphene Structure

The first step consists in calculating the conductivity of the graphene sheets that act as radiating elements. The complexity of the models used to this end will depend on the frequency band of interest and the characteristics of the graphene sheet, since they determine whether phenomena such as damping or the Hall effect should be taken into consideration [45], [46], [52]. The operating temperature, the chemical potential, the carrier mobility and the relaxation time of the graphene sample also need to be provided. Note that, as mentioned in Section II-B, the substrate on which the graphene layer will be placed may affect the value of the carrier mobility.

In this paper, we model and evaluate the graphenna shown in Fig. 5. Since the dimensions of the graphene patch are of a few micrometers (see Table 5) and its expected radiation frequency lies within the range where the intraband conductivity dominates, we can use (1) to obtain $\sigma(\omega)$.

B. Obtaining the Impulse Response Through Simulation

Once the frequency-dependent conductivity of graphene is calculated, the radiating element of the antenna can be rigorously modeled as an infinitesimally thin surface with an equivalent impedance of $Z(\omega) = \frac{1}{\sigma(\omega)}$. The graphene layer needs to be shaped according to antenna geometry and then integrated with the substrate, the feed, the ground plane, or any other component that may be present in the target antenna configuration. Among other parameters, the dimensions and permittivity of the substrate, as well as the type of source and its impedance need to be defined since they determine the performance of the resulting graphenna and, by extension, its impulse response. The complexity and accuracy of the model used to describe the antenna is a design decision and will depend on the focus of the study.

Two different methods can be followed to obtain the response of the antenna by means of an electromagnetic simulator. Provided that a feeding mechanism is defined, the simulator will calculate the fields radiated by the antenna as a function of the input voltage in transmission. Reciprocally, simulators generally allow to consider a wave incident to the antenna to then calculate the voltage at the antenna terminals in reception. In both cases, the response of the antenna can be derived in the time domain by relating the voltage and electromagnetic field using (5)-(7), or in the frequency domain using (6)-(8). The domain depends on the numerical method used to simulate the performance of the antenna; simulators commonly offer methods in both domains [53].

In case the response is calculated in the frequency domain, it is necessary to apply the inverse Fourier transform to obtain the impulse response:

$$h(t) = \mathcal{F}^{-1}(H(\omega)) = \int_{-\infty}^{\infty} H(\varepsilon) e^{2\pi i \varepsilon t} d\varepsilon. \tag{9}$$

Note that the frequency response needs to be defined over all frequencies, so that limiting the band will introduce errors in the inverse transform if the response is non-zero outside the band of interest. These errors will have an impact upon the performance metrics that only depend on the impulse response of the antenna. However, this fact does not truly affect the study of the communication performance of any antenna provided that the transmitted signals will be band-pass and within the band of interest.

In this paper, we use FEKO [53] to evaluate the family of graphennas shown and described in Fig. 5. We chose a very simple configuration without ground plane and where the air serves as substrate to focus on the methodological

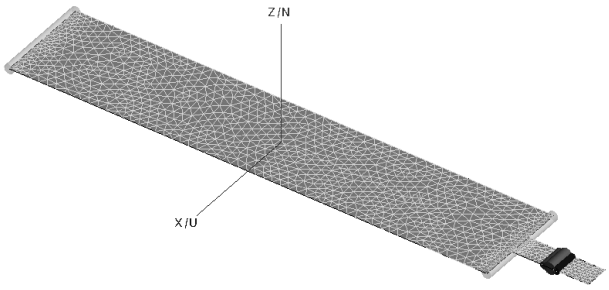

(a)

Width (W)	5 μm
Length (L)	1 μm
Chemical Potential (E_F)	0.1 - 2 eV
Carrier Mobility (μ)	0.5 - 6 $m^2V^{-1}s^{-1}$
Feed Type	Microstrip
Source Impedance (Z_{TX})	10 $k\Omega$
Substrate	Air (freestanding)
Frequency Range	0.1 - 10 THz
Input Pulse Types	Gaussian, Sinc
Input Pulse Bandwidth	100 GHz

(b)

Fig. 5. (a) Schematic diagram and (b) characteristics of the family of graphennas under investigation.

details rather than on the antenna design. However, it is worth reminding that the methodology is applicable to more complex and realistic antennas such as the ones proposed in related work. In our case, we evaluate the frequency response of the antenna in the band of interest (0.1 - 10 THz) and we then apply the inverse Fourier transform to it. Although limiting the spectrum is expected to generate an error due to non-zero response at optical frequencies, the consequences will be minor by virtue of the low conductivity value at such high frequency band (see Section II-A). Finally, it is worth noting that the feed impedance takes a constant value of 10 $k\Omega$. This is due to the high impedance of graphene antennas, which is typically of up to a few $k\Omega$ and suggests the use of high-impedance sources such as photomixers to reduce the impedance mismatch [42], [43] . Since $h(t)$ models, among other effects, the impedance mismatch between the antenna and the source, varying the source impedance will potentially impact upon any graphenna performance metric.

C. Characterizing the Antenna in the Time Domain

The final step in our methodology is to employ the impulse response $h(t)$ to fully characterize the antenna. This process is independent of whether the antenna is metallic or graphene-based and requires a set of performance metrics different from the ones used in narrowband systems. In this work, we will use the family of metrics proposed in [51], [54], the majority of which are calculated by means of the analytic response:

$$h^+(t) = h(t) + j\mathcal{H} \tag{10}$$

where $\mathcal{H}$ is the Hilbert transform of the impulse response. The reason behind the choice of the analytic response is that its envelope $|h^+(t)|$ is a faithful representation of the dispersion of the antenna since it gives insight into how the energy input to the antenna is distributed over time.

There are two aspects that are worth noting in order to justify the use of time-domain metrics and to better understand their meaning. On the one hand, pulse-based modulations have been proposed as the fundamental mechanism for communication among nanosystems [9]. On the other hand, area and complexity requirements suggests that non-coherent receivers, which are only capable of extracting information from the power of the signal, may be the only feasible option to demodulate the data [55], [56]. Within this context, the main objective is to maximize the power that reaches the receiver (to reduce the error rate) while minimizing the broadening of pulses (to increase the data rate). Both goals are modeled through the following metrics:

Response Peak the peak p of the antenna response is defined as the maximum value of the envelope of the analytic response:

$$p = \max_t |h^+(t)|^2. \tag{11}$$

A high peak value could mean that the energy is highly concentrated around a given time instant. Receiving a strong peak allows for a precise detection of the pulse position, which is desirable in location and ranging applications, as well as in coherent communication systems. In the case of non-coherent communication, a high peak value is not necessarily a decisive factor since the receiver accounts for the energy in a time interval that may span the whole received pulse.

Peak Width: one way to evaluate the width τ_W of the antenna response is by calculating the Full Width at Half Maximum (FWHM) of the envelope of the analytic response; this is, the difference between the time instants wherein such magnitude is half of the maximum:

$$\tau_W = t_{h2} - t_{h1} \tag{12}$$

where $t_{h1} = t'$ so that $|h^+(t')| = p/2$, and $t_{h2} = t''$ so that $t'' > t_{h1} \wedge |h^+(t'')| = p/2$.

The envelope width is a clear indicator of the dispersion introduced by the antenna. The lower is this value, the lower is the broadening that pulses will suffer. In this case, the inter-pulse interval could be reduced leading to higher data rates.

Ringing Duration: the ringing duration τ_R is generally defined with respect to a parameter α that represents the portion of ringing energy that can be considered negligible. We express the ringing duration as the time interval between the response peak and the antenna response reaching the upper bound of its normalized cumulative energy function, defined by α:

$$\tau_R(\alpha) = t_\alpha - t_p \tag{13}$$

where $t_p = t'$ so that $|h^+(t')| = p$ and $t_\alpha = t''$ so that $t'' > t_p \wedge |h^+(t'')| = \alpha \cdot p$.

The ringing phenomenon is accumulated in the tail of the transmitted pulse and is generally due to resonances caused by energy storage or multiple reflections within the radiating structure [51]. For high data rates, the ringing of a given pulse may overlap with the following symbol, causing a raise of the inter-symbol interference and therefore limiting the maximum achievable data rate of the transmission. Hence, a low ringing duration is desirable.

Transient Gain: the transient gain g_T is the time domain version of the antenna gain. It is defined as the ratio of the radiation intensity of the antenna, $U_{rad} = r^2 \frac{\|e_{TX}(t)\|^2}{Z_0}$, to the radiation intensity of an isotropic radiator, $U_{rad}^{iso} = \frac{P_{in}}{4\pi} = \frac{\|u_{TX}(t)\|^2}{4\pi Z_{TX}}$ with u_{TX} as the input voltage. Applying such definition, we obtain:

$$g_T(u_{TX}) = \frac{\|h(t) * \frac{\partial u_{TX}(t)}{\partial t}\|^2}{\|\sqrt{\pi} c_0 u_{TX}(t)\|^2}, \tag{14}$$

where the norm is $\|f(x)\| = \int_{-\infty}^{\infty} |f(x)| dx$. This time-domain gain can be also calculated in the frequency domain by using the Parseval Theorem, which states that the energy of a signal is the same both in the time and frequency domain ($\|h(t)\|^2 = \|H(\omega)\|^2$). Hence:

$$g_T(u_{TX}) = \frac{\|H(\omega) \cdot jw U_{TX}(f)\|^2}{\|\sqrt{\pi} c_0 U_{TX}(f)\|^2}. \tag{15}$$

The transient gain is an indicator of how efficiently an antenna is able to radiate a given input signal u_{TX}. It is specially relevant since the energy that will reach the receiver may be sparse due to both the expected high attenuation introduced by the channel and the transmitter limitations in terms of instantaneous power.

Pulse Width Stretch Ratio: similarly to the transient gain, the stretch ratio SR is defined with respect an input waveform. Let the normalized cumulative energy function of a given signal $s(t)$ be defined as:

$$E_s(t) = \frac{\int_{-\infty}^{t} |s(t)|^2}{\|s(t)\|^2}. \tag{16}$$

Assuming that a certain fraction α of ringing energy can be neglected, the width of the signal $W(s)$ can be then obtained with the following equation:

$$W(s) = E_s^{-1}(1 - \alpha/2) - E_s^{-1}(\alpha/2). \tag{17}$$

The stretch ratio is obtained by dividing the width of the radiated pulse by the width of the input waveform [54]:

$$SR(u_{TX}) = \frac{W(h * \frac{\partial u_{TX}}{\partial t})}{W(u_{TX})}. \tag{18}$$

Therefore, the pulse width stretch ratio quantifies the broadening of a pulse caused by the antenna. Note that values lower than 1 are possible, which do not imply that the output pulse is shorter than the input signal, but that antenna concentrates a significant fraction of the output pulse energy around the peak. A value close to 1 or below is desired, which means that the antenna has a nearly flat response in the frequency band of the input signal. Otherwise, the pulse width would increase leading to reduced transmission data rates.

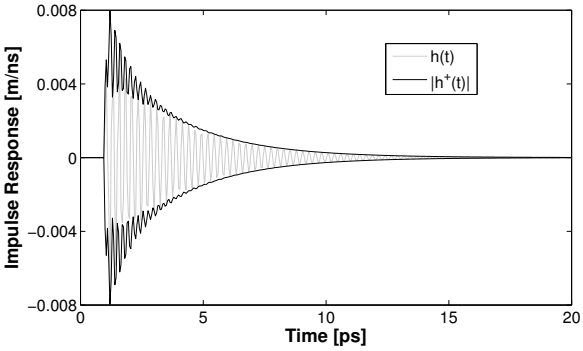

(a)

Response Peak	0.008 m/ns
Peak Width	1.5 ps
Ringing Duration ($\alpha = 10\%$)	5.65 ps
Transient Gain (Gaussian)	-9.32 dBi
Transient Gain (Sinc)	-9.495 dBi
Stretch Ratio (Gaussian, $\alpha = 10\%$)	1.103
Stretch Ratio (Sinc, $\alpha = 10\%$)	1.044

(b)

Fig. 6. (a) Impulse Response and (b) performance metrics of a 5µm × 1µm graphenna with a chemical potential of 0.5 eV and a carrier mobility of 60000 $cm^2V^{-1}s^{-1}$, which results in a relaxation time of 3 ps.

IV. Results

With the methodology explained in Section III-B, the graphenna under investigation (see Fig. 5) is characterized in the time domain considering the carrier mobility and the chemical potential as design space exploration variables. Note that, as specified in Section II-B, carrier mobility and relaxation time are interchangeable as parameters in the terahertz band.

A. Characterization of a Graphenna

Fig. 6a plots the impulse response of a graphenna under investigation with carrier mobility μ = 60000 $cm^2V^{-1}s^{-1}$ and chemical potential E_F = 0.5 eV (τ = 3 ps). The envelope of its analytic representation is also shown; both plots are delayed 1ps for the sake of clarity. The envelope of the analytic response increases at that point, rapidly reaching the response peak, and then an apparently exponential decay follows. Ringing effects cause oscillations to appear in the analytic response after the main peak and broaden the impulse response. It is worth noting that since the frequency response of the antenna over 10 THz has been ignored, a very high frequency component should be added to the impulse response shown in

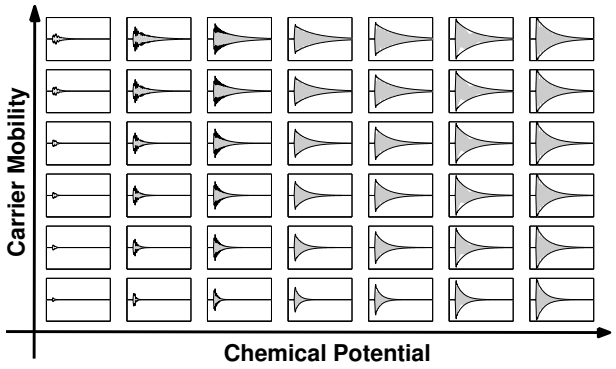

Fig. 7. Impulse Response matrix of 5μm × 1μm graphennas for a design space exploration with different carrier mobility (5000 - 60000 $cm^2V^{-1}s^{-1}$) and chemical potential (0.1 - 2 eV) values. The time interval ranges from 0 to 10 picoseconds.

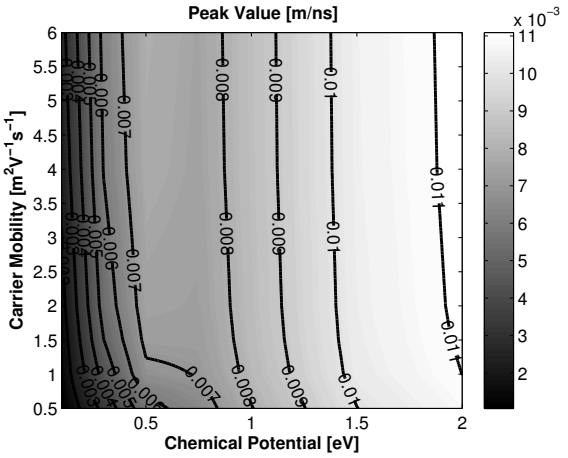

Fig. 8. Response peak as a function of the carrier mobility and chemical potential.

Fig. 6. However, the error is considered negligible given the very low value of the conductivity at optical frequencies.

Table 6b summarizes the performance of this specific graphenna with the metrics defined in Section III-C. For this configuration, the use of a gaussian pulse yields a slightly better gain, whereas employing a sinc pulse results in improved stretch ratio figures.

B. Design Space Exploration

In order to investigate the impact of the carrier mobility and chemical potential on the time-domain behavior of graphennas, we obtained the impulse response of a set of different graphennas within the parametric design space. Even though carrier mobilities of a few hundred thousands of $cm^2V^{-1}s^{-1}$ have been measured in nearly ideal conditions [47], we will evaluate a more conservative range between 5000 and 60000 $cm^2V^{-1}s^{-1}$, proved achievable with current graphene manufacturing techniques [32]. In the case of the chemical potential, typical values between 0.1 and 2 eV are considered, which are below the graphene electrical breakdown [57], [58]. The resulting relaxation time ranges from 0.05 to 12 ps in the frequency band of interest.

Fig. 7 shows the matrix of impulse responses, wherein each row and column corresponds to a chemical potential and carrier mobility value, respectively. The time interval is fixed and ranges from 0 to 10 picoseconds in all cases, whereas the vertical axis limits are also fixed to $[-P, P]$, where P is the maximum envelope peak among all the temporal responses.

In very low chemical potential and carrier mobility conditions, almost null impulse responses are obtained. This implies that resonance is not achieved due to the attenuation of SPP waves as they propagate on the surface of the graphenna. In order to obtain a non-negligible resonant behavior, such effects must be reduced by means of improving either the chemical potential or the carrier mobility. As mentioned in Section II-B, this increases the relaxation time of the material and leads to a stronger radiated field.

Although both the increase of the chemical potential and of the carrier mobility contribute to a raise of the radiated energy, the impact on the impulse response is different in each case. On the one hand, the energy variation observed as we modify the chemical potential is evenly distributed along the response, impacting both the response peak and pulse width. Such behavior matches the frequency-domain results (see Fig. 3a), which point towards an increase in the radiated signal strength. On the other hand, a similar effect is found when the carrier mobility is modified. However, the increase in radiated energy affects the width of the response and the ringing tail rather than the pulse amplitude. Such broadening of the temporal response is coherent with the sharpening of the resonant behavior that is observed when the carrier mobility is improved (see Fig. 3b).

The behavior of graphennas is further analyzed in the following paragraphs, wherein the impact of both the carrier mobility and the chemical upon the performance metrics presented in Section III-C is discussed. The main aim is to provide a quantification of such behavior and to bridge it to relevant aspects regarding the impulse radio communications application.

Response Peak: Fig. 8 shows the results regarding the response peak, as functions of both the carrier mobility and the chemical potential. The results therein confirm that the peak value is clearly proportional to the chemical potential since contour lines are parallel to the Y-axis. The weak dependence shown with respect to the carrier mobility confirms that the raise in antenna efficiency impacts on the impulse response width and ringing length rather than on the peak value.

Peak Width: Fig. 9a plots the peak width as a function of both the carrier mobility and the chemical potential. Narrow responses are obtained for low chemical potentials and carrier mobilities. The peak width then sharply increases with the chemical potential for values up to approximately 1 eV and with the carrier mobility. When the chemical potential surpasses 1 eV, the peak width plateaus or slightly decreases depending on the carrier mobility value. This behavior can be explained as follows: the response becomes wider with the carrier mobility due to the increase of ringing effects clearly observed in Fig. 7. However, the specific impact upon the response width depends on the value of the half-maximum: at

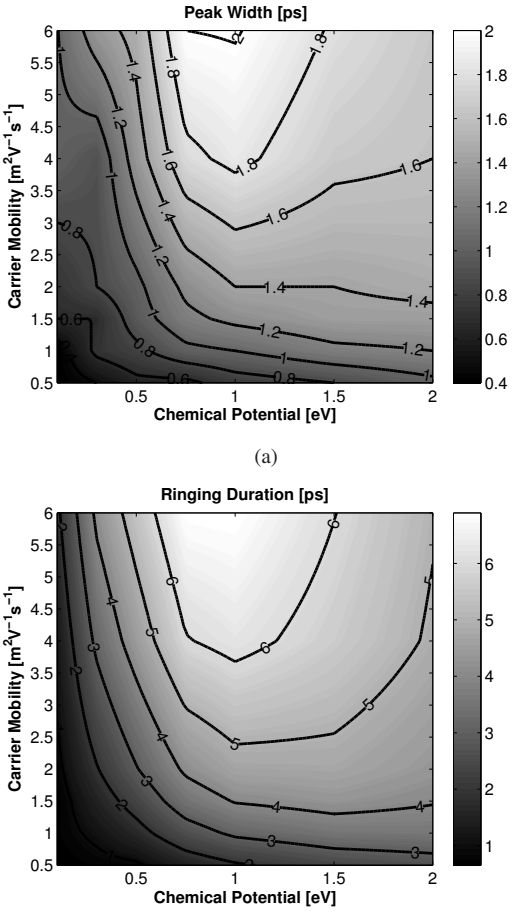

Fig. 9. (a) Peak width and (b) ringing duration ($\alpha = 10\%$) as functions of the carrier mobility and chemical potential.

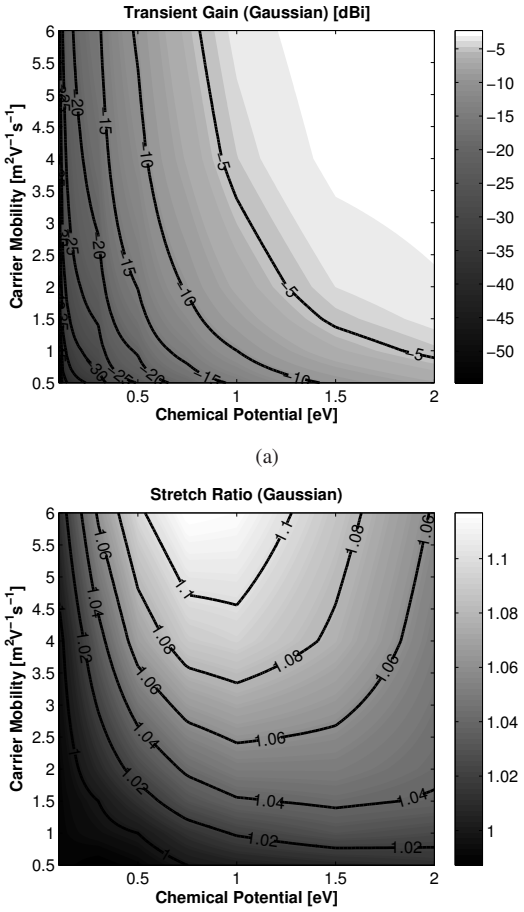

Fig. 10. (a) Transient gain and (b) stretch ratio as functions of the relaxation time and chemical potential, assuming a gaussian pulse as input.

low chemical potentials, the peak value is low and therefore ringing effects dominate; whereas at high chemical potentials, the peak value is high and the impact of incremental ringing diminishes.

Ringing Duration: Fig. 9b shows the ringing duration as a function of both the carrier mobility and the chemical potential, assuming $\alpha = 10\%$. Two main tendencies are clearly observed regarding the ringing duration: first, that it increases with the carrier mobility and, second, that its dependence on the chemical potential is rather parabolic as it increases until approximately E_F = 1 eV and then moderately decreases. The highest ringing values are therefore obtained with the combination of high carrier mobilities and E_F = 1 eV. Since the ringing duration also depends on the peak value, a similar reasoning to that of the peak width can be made to explain this behavior.

Transient Gain: Fig. 10a shows the transient gain as functions of both the carrier mobility and the chemical potential when a gaussian pulse is radiated. The results therein indicate that both technological parameters have a similar impact upon the transient gain for this test signal. Such behavior matches the results observed in Fig. 7, which show an increase in terms of impulse response in the presence of high chemical potential and carrier mobilities. Apparently, whether this such energy surge revolve around the response peak or not does not make a difference when evaluating the transient gain for this test signal. However, this tendency may vary when changing the bandwidth of the input signal. The same analysis has been also performed using a sinc function with the same bandwidth and energy, showing identical tendencies with very similar absolute values.

Pulse Width Stretch Ratio: Fig. 10b shows the pulse width stretch ratio as a function of both the carrier mobility and the chemical potential, assuming a gaussian pulse as input. The trend shown therein is similar to that of the ringing. A clear and undesired rise of the stretch ratio is observed when the chemical potential is increased below 0.9 eV, with a particularly strong transition around 0.5 eV and high carrier mobilities. After reaching its highest value, the stretch ratio moderately decreases for both high carrier mobilities and high chemical potentials. The same relative behavior is observed when a sinc-shaped pulse is used as input, but with a general improvement in absolute terms.

C. Comparison with Gold Antennas

In order to complete the analysis, Table I shows a comparison between two graphennas with different carrier mobility and chemical potential values, along with two different

TABLE I
COMPARISON OF THE PERFORMANCE METRICS OF DIFFERENT METALLIC AND GRAPHENE-BASED ANTENNAS.

	Graphenna 1 E_F=0.1, μ=6	Graphenna 2 E_F=2, μ=1	Gold Antenna 1	Gold Antenna 2
Area	5 μm^2	5 μm^2	1125 μm^2	5 μm^2
f_{res}	1.74 THz	7.48 THz	1.52 THz	22.5 THz
p	0.003 m/ns	0.01 m/ns	0.12 m/ns	0.04 m/ns
τ_W	1 ps	1.2 ps	0.45 ps	0.06 ps
$\tau_R(10\%)$	1.95 ps	3.6 ps	1 ps	0.1 ps
$g_{T,G}$	-31.56 dBi	-4.55 dBi	-8.17 dBi	-9.45 dBi
SR_G	1.013	1.026	0.9957	0.9843
$g_{T,S}$	-31.6 dBi	-4.623 dBi	-8.19 dBi	-9.45 dBi
SR_S	0.9912	1	0.9912	0.9888

metallic antennas: a micrometric patch, which has a resonant frequency of several tens of terahertz; as well as a metallic patch resonating in a similar frequency band than the graphennas. The metrics $g_{T,G}$, SR_G and $g_{T,S}$, SR_S correspond to the transient gain and stretch ratio for a gaussian pulse and a sinc-shaped pulse centered at the resonant frequency of each considered antenna. Note that since the impedance of gold antennas is in the order of 100Ω, we will use a 75-Ω source impedance to drive the antenna in these cases for the sake of fairness.

In order to reach the same resonant frequency than a graphenna, a gold patch is approximately two orders of magnitude larger in terms of area. Moreover, the patch is 0.5 μm thick (gold cannot be infinitesimally thin). This size difference allows this antenna to radiate more energy, resulting in a higher envelope peak. However, it is observed that this fact does not ensure the best performance in terms of relative radiation efficiency (transient gain). The response of the 75μm × 15μm gold patch is the narrowest among the compared antennas, which allows it to perform remarkably well in terms of stretch ratio. The second gold antenna, the dimensions of which are comparable to that of the graphennas (but 0.033-μm thick), resonates at a much higher frequency than the other antennas. In this case, the gold antenna shows an outstanding performance in terms of response width and ringing, leading to the lowest stretch ratio figures. Although remarkable performance is observed in terms of envelope peak, the reduced transient gain implies that graphennas of the same size will be able to radiate with higher efficiency.

In light of these results, it is reasonable to conclude that even though gold antennas show an slightly improved potential performance, the difference will be compensated by the unique size and resonant frequency characteristics of graphennas.

D. Figure of Merit Proposal

The metrics analyzed in the previous sections summarize the performance of graphennas in terms of how the input energy will be distributed among time and radiated. This includes two main aspects, namely, *(a)* the quantity of energy that will be effectively radiated and *(b)* the interval of time required by the graphenna to radiate a high percentage of such quantity. We have observed that these may depend on the signal with which the graphenna is fed: the quantity of energy is related to the transient gain, whereas the time interval is related with the pulse width stretch ratio. From a communications standpoint, both parameters are of special importance since they impact the quality of the communication as follows:

- The energy that will reach the receiver is expected to be low due both to the instantaneous power limitations at the transmitter and to the expected high path loss. The lower such energy, the higher the probability of incorrectly decoding the transmitted bit at the receiver will be. This situation may force the system to operate at lower data rates in order to maintain an acceptable bit error rate. In this context, the alternative is to optimize the transient gain of the antenna so that the radiated energy is maximized.
- The data rate in pulse-based modulations (proposed as fundamental communication mechanism among nanosytems [9]) is inversely proportional to the inter-symbol interval. Such parameter is generally lower-bounded by the width of the radiated pulse in order to avoid inter-symbol interference at the receiver, limiting the data rate. In other words, the higher the pulse width at the output of the antenna, the lower the data rate will be. Therefore, it is desirable to optimize the stretch ratio of the antenna to maximize the data rate.

The reader will observe in Fig. 10 that the transient gain and the stretch ratio follow roughly inverse trends, so that the optimization of the transient gain may not ensure an acceptable stretch ratio and *vice versa*. In order to capture this tradeoff, we propose the employment of a figure of merit that encompasses both metrics:

$$FoM(u_{TX}) = \left.\frac{g_T}{SR}\right|_{u_{TX}}, \tag{19}$$

with g_T given by (15) and SR given by (18), both particularized for an input signal u_{TX}. A high value of this figure of merit implies both that the transient gain is high and that the stretch ratio is low for a given input signal, leading to increased data rates with acceptable bit error probabilities. This way, specific transceivers could be devised through a transmitter and graphenna co-design process, aiming at jointly optimizing both metrics.

Fig. 11 shows the proposed figure of merit for graphennas as functions of their carrier mobility and chemical potential, assuming a gaussian pulse as input. The tendencies observed indicate that graphennas show a better energy-data rate joint performance for both high carrier mobility and chemical potential values, at least for a gaussian pulse. This tendency basically implies that the pulse broadening observed when the carrier mobility increases is largely compensated with a consistent growth in transient gain obtained when both technological parameters are increased. Note, though, that this tendency may vary when changing the bandwidth or shape of the input signal.

V. CONCLUSIONS

A framework for the time-domain characterization of graphene-based miniaturized antennas, or *graphennas*, has been presented. The methodology follows an extremely

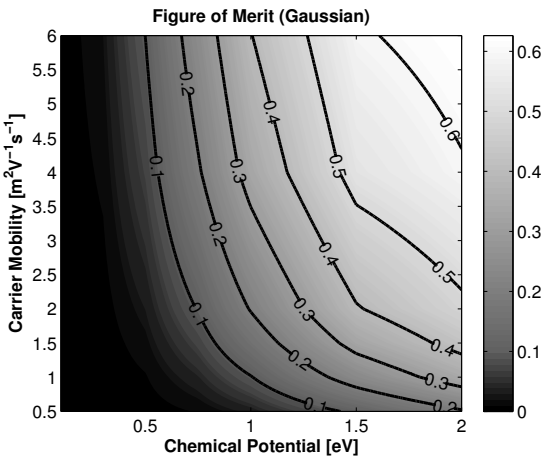

Fig. 11. Figure of Merit as a function of the relaxation time and chemical potential, assuming a gaussian input.

vertical approach, encompassing *(a)* the modeling of the graphenna, including its unique plasmonic effects, as a function of technological design aspects such as quality of the material, i.e. the carrier mobility, or the chemical potential applied to the antenna; *(b)* the simulation of the graphenna using finite element field solvers, and *(c)* the obtainment of key time-domain characteristics through a set of performance metrics. Such verticality enables the exploration of the design space delimited by the key technological parameters of graphene, in the pathway to find the most suitable graphenna for communication purposes. A 5μm × 1μm graphene-based patch antenna has been analyzed using this methodology and then benchmarked against representative gold antennas. From the results, it is concluded that the graphenna shows performance levels comparable to that of metallic antennas. The analysis also reveals a tradeoff between radiation efficiency and pulse dispersion in graphennas, which is captured in a proposed figure of merit. Since it is dependent on the pulse to be radiated, such figure of merit could be used to optimize the communications performance by means of a transmitter and graphenna co-design process.

ACKNOWLEDGMENT

The authors would like to thank the reviewers for their valuable comments and suggestions which helped to improve the quality of the paper.

REFERENCES

[1] I. F. Akyildiz, J. M. Jornet, and M. Pierobon, "Nanonetworks: A New Frontier in Communications," *Communications of the ACM*, vol. 54, no. 11, p. 84, Nov. 2011.

[2] S. Deb, A. Ganguly, P. P. Pande, B. Belzer, and D. Heo, "Wireless NoC as Interconnection Backbone for Multicore Chips: Promises and Challenges," *IEEE Journal on Emerging and Selected Topics in Circuits and Systems*, vol. 2, no. 2, pp. 228–239, 2012.

[3] I. F. Akyildiz and J. M. Jornet, "Electromagnetic Wireless Nanosensor Networks," *Nano Communication Networks (Elsevier) Journal*, vol. 1, no. 1, pp. 3–19, 2010.

[4] ——, "The Internet of nano-things," *Wireless Communications, IEEE*, vol. 17, no. 6, pp. 58–63, 2010.

[5] M. Walther, D. Cooke, C. Sherstan, M. Hajar, M. Freeman, and F. Hegmann, "Terahertz conductivity of thin gold films at the metal-insulator percolation transition," *Physical Review B*, vol. 76, no. 12, p. 125408, 2007.

[6] S. Abadal, E. Alarcón, M. C. Lemme, M. Nemirovsky, and A. Cabellos-Aparicio, "Graphene-enabled Wireless Communication for Massive Multicore Architectures," *IEEE Communications Magazine*, vol. 51, no. 11, pp. 137–143, 2013.

[7] I. Akyildiz, J. Jornet, and C. Han, "TeraNets: ultra-broadband communication networks in the terahertz band," *IEEE Wireless Communications*, vol. 21, no. 4, pp. 130–135, 2014.

[8] J. M. Jornet and I. F. Akyildiz, "Graphene-based nano-antennas for electromagnetic nanocommunications in the terahertz band," in *Proceedings of the EuCAP '10*, 2010, pp. 1–5.

[9] ——, "Femtosecond-Long Pulse-Based Modulation for Terahertz Band Communication in Nanonetworks," *IEEE Transactions on Communications*, vol. 62, no. 5, pp. 1742 – 1754, 2014.

[10] R. G. Cid-fuentes, J. M. Jornet, I. F. Akyildiz, and E. Alarcón, "A Receiver Architecture for Pulse-based Electromagnetic Nanonetworks in the Terahertz Band," in *Proceedings of the ICC '12*, 2012, pp. 4937–4942.

[11] I. Llatser, C. Kremers, D. Chigrin, J. M. Jornet, M. C. Lemme, A. Cabellos-Aparicio, and E. Alarcón, "Radiation Characteristics of Tunable Graphennas in the Terahertz Band," *Radioengineering Journal*, vol. 21, no. 4, 2012.

[12] M. Tamagnone, J. S. Gómez-Díaz, J. Perruisseau-Carrier, and J. R. Mosig, "High-impedance frequency-agile THz dipole antennas using graphene," in *Proceedings of the EuCAP '13*, 2013, pp. 533–536.

[13] M. Tamagnone, J. S. Gomez-Diaz, J. R. Mosig, and J. Perruisseau-Carrier, "Analysis and design of terahertz antennas based on plasmonic resonant graphene sheets," *Journal of Applied Physics*, vol. 112, p. 114915, 2012.

[14] Y. Huang, N. Khiabani, Y. Shen, and D. Li, "Terahertz photoconductive antenna efficiency," in *Proceedings of the iWAT '11*, 2011, pp. 152–56.

[15] J. M. Jornet and I. F. Akyildiz, "Graphene-based Plasmonic Nano-Antenna for Terahertz Band Communication in Nanonetworks," *IEEE Journal on Selected Areas in Communications*, vol. 31, no. 12, pp. 685–694, Dec. 2013.

[16] I. Llatser, C. Kremers, and A. Cabellos-Aparicio, "Scattering of terahertz radiation on a graphene-based nano-antenna," in *Proc. of the Fourth International Workshop on Theoretical and Computational Nano-Photonics*, vol. 1938, Bad Honnef, Germany, 2011, pp. 144–146.

[17] I. Llatser, C. Kremers, A. Cabellos-Aparicio, J. M. Jornet, E. Alarcón, and D. N. Chigrin, "Graphene-based nano-patch antenna for terahertz radiation," *Photonics and Nanostructures - Fundamentals and Applications*, vol. 10, no. 4, pp. 353–358, 2012.

[18] M. Dragoman, A. A. Muller, D. Dragoman, F. Coccetti, and R. Plana, "Terahertz antenna based on graphene," *Journal of Applied Physics*, vol. 107, p. 104313, 2010.

[19] M. Tamagnone, J. S. Gomez-Diaz, J. R. Mosig, and J. Perruisseau-Carrier, "Reconfigurable terahertz plasmonic antenna concept using a graphene stack," *Applied Physics Letters*, vol. 101, p. 214102, 2012.

[20] J. Perruisseau-Carrier, "Graphene for antenna applications: Opportunities and challenges from microwaves to THz," in *Proceedings of the LAPC '12*. Ieee, Nov. 2012, pp. 1–4.

[21] M. Liang, M. Tuo, S. Li, Q. Zhu, and H. Xin, "Graphene Conductivity Characterization At Microwave and THz Frequency," in *Proceedings of the EuCAP '14*, 2014, pp. 489–491.

[22] T. Zhou, Z. Cheng, H. Zhang, M. L. Berre, L. Militaru, and F. Calmon, "Miniaturized Tunable Terahertz Antenna Based on Graphene," *Microwave and Optical Technology Letters*, vol. 56, no. 8, pp. 1792–1794, 2014.

[23] S. Amanatiadis and N. Kantartzis, "Design and analysis of a gate-tunable graphene-based nanoantenna," in *Proceedings of the EuCAP '13*, 2013, pp. 4038–4041.

[24] A. S. Thampy, M. S. Darak, and S. K. Dhamodharan, "Analysis of graphene based optically transparent patch antenna for terahertz communications," *Physica E: Low-dimensional Systems and Nanostructures*, vol. 66, no. February, pp. 67–73, Oct. 2015.

[25] M. Tamagnone, J. S. Gómez-Díaz, J. Mosig, and J. Perruisseau-Carrier, "Hybrid graphene-metal reconfigurable terahertz antenna," in *Proceedings of the IMS '13*, 2013, pp. 9–11.

[26] B. Gulbahar and O. B. Akan, "A Communication Theoretical Modeling of Single-Layer Graphene Photodetectors and Efficient Multireceiver Diversity Combining," *IEEE Transactions on Nanotechnology*, vol. 11, no. 3, pp. 601–610, 2012.

[27] M. Kuscu, "An Information-Theoretic Model and Analysis of Graphene Plasmon-Assisted FRET-Based Nanocommunication Channel," in *Proceedings of the NANOCOM '14*, 2014.
[28] A. K. Geim and K. S. Novoselov, "The rise of graphene," *Nature materials*, vol. 6, no. 3, pp. 183–191, Mar. 2007.
[29] F. Schwierz, "Graphene transistors," *Nature nanotechnology*, vol. 5, no. 7, pp. 487–96, Jul. 2010.
[30] X. Wang, L. Zhi, and K. Müllen, "Transparent, conductive graphene electrodes for dye-sensitized solar cells," *Nano Letters*, vol. 8, no. 1, pp. 323–7, 2008.
[31] A. Vakil and N. Engheta, "Transformation optics using graphene," *Science*, vol. 332, no. 6035, pp. 1291–4, 2011.
[32] M. Jablan, H. Buljan, and M. Soljačić, "Plasmonics in graphene at infrared frequencies," *Physical review B*, vol. 80, no. 24, p. 245435, 2009.
[33] F. H. L. Koppens, D. E. Chang, and F. J. G. D. Abajo, "Graphene Plasmonics : A Platform for Strong Light-Matter Interactions," *Nano Letters*, pp. 3370–3377, 2011.
[34] Z. Fei, A. S. Rodin, G. O. Andreev, W. Bao, A. S. McLeod, M. Wagner, L. M. Zhang, Z. Zhao, M. Thiemens, G. Dominguez, M. M. Fogler, A. H. C. Neto, C. N. Lau, F. Keilmann, and D. N. Basov, "Gate-tuning of graphene plasmons revealed by infrared nano-imaging," *Nature*, vol. 487, pp. 82–85, 2012.
[35] G. Hanson, "Fundamental transmitting properties of carbon nanotube antennas," *IEEE Transactions on Antennas and Propagation*, vol. 53, no. 11, pp. 3426–3435, 2005.
[36] P. J. Burke, S. Li, and Z. Yu, "Quantitative Theory of Nanowire and Nanotube Antenna Performance," *IEEE Transactions on Nanotechnology*, vol. 5, no. 4, pp. 314–334, 2006.
[37] K. Kempa, J. Rybczynski, Z. Huang, K. Gregorczyk, A. Vidan, B. Kimball, J. Carlson, G. Benham, Y. Wang, A. Herczynski, and Z. F. Ren, "Carbon Nanotubes as Optical Antennae," *Advanced Materials*, vol. 19, no. 3, pp. 421–426, Feb. 2007.
[38] G. W. Hanson, "Dyadic Green's Functions for an Anisotropic , Non-Local Model of Biased Graphene," *IEEE Transactions on Antennas and Propagation*, vol. 56, no. 3, pp. 747–757, 2008.
[39] I. Llatser, C. Kremers, A. Cabellos-Aparicio, E. Alarcón, and D. N. Chigrin, "Comparison of the resonant frequency in graphene and metallic nano-antennas," *AIP Conference Proceedings*, vol. 1475, pp. 143–145, 2012.
[40] R. Singh, C. Rockstuhl, and C. Menzel, "Spiral-type terahertz antennas and the manifestation of the Mushiake principle," *Optics*, vol. 17, no. 12, pp. 9971–9980, 2009.
[41] X. Zhang, G. Auton, E. Hill, and Z. Hu, "Graphene THz Ultra Wideband CPW-fed Monopole Antenna," in *1st IET Colloquium on Antennas, Wireless and Electromagnetics*, 2013.
[42] A. Cabellos, I. Llatser, E. Alarcón, A. Hsu, and T. Palacios, "Use of THz Photoconductive Sources to Characterize Tunable Graphene RF Plasmonic Antennas," *IEEE Transactions on Nanotechnology*, vol. PP, no. 99, Jan. 2014.
[43] M. Tamagnone and J. Perruisseau-carrier, "Predicting Input Impedance and Efficiency of Graphene Reconfigurable Dipoles Using a Simple Circuit Model," *IEEE Antennas and Wireless Propagation Letters*, vol. 13, pp. 313–316, 2014.
[44] C. H. Gan, H. S. Chu, and E. P. Li, "Synthesis of highly confined surface plasmon modes with doped graphene sheets in the midinfrared and terahertz frequencies," *Physical Review B*, vol. 85, no. 12, p. 125431, Mar. 2012.
[45] A. H. Castro Neto, F. Guinea, N. M. R. Peres, K. S. Novoselov, and A. K. Geim, "The electronic properties of graphene," *Reviews of Modern Physics*, vol. 81, no. 1, pp. 109–162, Jan. 2009.
[46] F. Bonaccorso, Z. Sun, T. Hasan, and A. C. Ferrari, "Graphene Photonics and Optoelectronics," *Nature Photonics*, vol. 4, pp. 611–622, Jun. 2010.
[47] K. I. Bolotin, K. J. Sikes, Z. Jiang, M. Klima, G. Fudenberg, J. Hone, P. Kim, and H. L. Stormer, "Ultrahigh electron mobility in suspended graphene," *Solid State Communications*, vol. 146, pp. 351–355, 2008.
[48] H. Hirai, H. Tsuchiya, Y. Kamakura, N. Mori, and M. Ogawa, "Electron mobility calculation for graphene on substrates," *Journal of Applied Physics*, vol. 116, no. 8, p. 083703, Aug. 2014.
[49] A. Shlivinski, E. Heyman, and R. Kastner, "Antenna characterization in the time domain," *IEEE Transactions on Antennas and Propagation*, vol. 45, no. 7, pp. 1140–1149, 1997.
[50] E. G. Farr and C. E. Baum, "Time Domain Characterization of Antennas with TEM Feeds," in *Sensor and Simulation Notes*, 1998, p. Note 426.
[51] W. Wiesbeck, G. Adamiuk, and C. Sturm, "Basic Properties and Design Principles of UWB Antennas," *Proceedings of the IEEE*, vol. 97, no. 2, pp. 372–385, Feb. 2009.
[52] K. S. Novoselov, S. V. Morozov, T. M. G. Mohinddin, L. a. Ponomarenko, D. C. Elias, R. Yang, I. I. Barbolina, P. Blake, T. J. Booth, D. Jiang, J. Giesbers, E. W. Hill, and a. K. Geim, "Electronic properties of graphene," *Physica Status Solidi (B)*, vol. 244, no. 11, pp. 4106–4111, Nov. 2007.
[53] "EM Software and Systems, FEKO." [Online]. Available: http://www.feko.info
[54] D.-H. Kwon, "Effect of Antenna Gain and Group Delay Variations on Pulse-Preserving Capabilities of Ultrawideband Antennas," *IEEE Transactions on Antennas and Propagation*, vol. 54, no. 8, pp. 2208–2215, Aug. 2006.
[55] S. Abadal, I. Llatser, A. Mestres, J. Solé-Pareta, E. Alarcón, and A. Cabellos-Aparicio, "Fundamentals of Graphene-enabled Wireless On-Chip Networking," in *Modeling, Methodologies and Tools for Molecular and Nano-scale Communication*. Springer, 2015.
[56] K. Witrisal, G. Leus, G. J. M. Janssen, M. Pausini, F. Troesch, T. Zasowski, and J. Romme, "Noncoherent ultra-wideband systems," *IEEE Signal Processing Magazine*, vol. 26, no. 4, pp. 48–66, 2009.
[57] S. Tongay, K. Berke, M. Lemaitre, Z. Nasrollahi, D. B. Tanner, A. F. Hebard, and B. R. Appleton, "Stable hole doping of graphene for low electrical resistance and high optical transparency," *Nanotechnology*, vol. 22, p. 425701, 2011.
[58] C. Xu, Y. Jin, L. Yang, J. Yang, and X. Jiang, "Characteristics of electro-refractive modulating based on Graphene-Oxide-Silicon waveguide," *Optics Express*, vol. 20, no. 20, pp. 22 308–22 405, 2012.

Sergi Abadal received the B.Sc. and M.Sc. degrees in telecommunication engineering from the Technical University of Catalunya (UPC), Barcelona, Spain, in 2010 and 2011, respectively, and is currently pursuing the Ph.D. degree in computer architecture at the NaNoNetworking Center in Catalunya, UPC. From 2009 to 2010, he was a Visiting Researcher with the Broadband Wireless Networking Laboratory, Georgia Institute of Technology, Atlanta, USA. His current research interests are ultra-high-speed on-chip wireless networks and broadcast-enabled manycore processor architectures. Mr. Abadal was awarded by INTEL within its Doctoral Student Honor Program in 2013.

Ignacio Llatser received a double degree in Telecommunication Engineering and Computer Science (2008), a Master degree in Computer Architecture, Networks and Systems (2011) and a Ph.D. degree in Computer Architecture (2014) from the Technical University of Catalunya (UPC), Barcelona, Spain. He is currently a postdoctoral researcher at the Technical University of Dresden, Germany, in the framework of the European project AutoNet2030. He has held several research appointments at the École Polytechnique Fédérale de Lausanne, Switzerland (2008), the Georgia Institute of Technology, USA (2011 and 2013) and the Bergische Universität Wuppertal, Germany (2012). His research interests lie in the fields of nanoscale communication networks, vehicular networks and autonomous driving.

Albert Mestres was born in Barcelona, Catalunya (Spain) in 1987. He received a double M.Sc. degree in Telecommunication Engineering and in Computer Science from Technical University of Catalunya (UPC), in 2012. From February 2011 to November 2011, he was a visiting researcher at the Broadband Wireless Networking Lab, Georgia Institute of Technology, Atlanta, USA. Since 2013, he is pursuing his Ph.D. at the NaNoNetworking Center in Catalunya, UPC. His current research interests are graphene-based wireless communications for on-chip networks.

Heekwan Lee received the B.Sc. degree in electrical engineering from Yonsei University, Seoul, Korea, in 1996, and the M.A. degree in mathematics and M.Sc. and Ph.D. degrees in electrical engineering from the University of Southern California (USC), Los Angeles, CA, USA, in 1999, 2001, and 2005, respectively. After his graduation, he joined the Samsung Advanced Institute of Technology, Suwon, Korea. Now he is working in DMC with Samsung Electronics. His current research interests include coding theory, cryptography, and information theory and security.

Eduard Alarcón (S'96, M'01), received M. Sc. (national award) and Ph.D. degrees in EE from UPC Barcelona, Spain, in 1995 and 2000, respectively, where he became Associate Professor in 2001, and has been visiting Professor at University of Colorado at Boulder, USA (2003, 2006, 2008) and KTH Stockholm (2011). He has coauthored more than 300 scientific publications, 8 book chapters and 8 patents, and has been involved in different national, EU and US R&D projects. Research interests include the areas of on-chip energy management circuits, energy harvesting and wireless energy transfer, nanocommunications and small satellites. He has been funded and awarded several research projects by companies including Google, Samsung and Intel. He has given 30 invited lectures and tutorials worldwide. He is Vice President of the IEEE CAS society, was elected member of the IEEE CAS Board of Governors (2010-2013) and was IEEE CAS society distinguished lecturer, recipient of the Best paper award at IEEE MWSCAS98, co-editor of 6 journal special issues, 8 conference special sessions, TPC co-chair and TPC member of 30 IEEE conferences, and Associate Editor for IEEE TCAS-I, TCAS-II, JETCAS, JOLPE and Nano Communication Networks.

Albert Cabellos-Aparicio received the B.Sc., M.Sc., and Ph.D. degrees in computer science engineering from the Technical University of Catalunya, Barcelona, Spain, in 2001, 2005, and 2008, respectively. He has also been an Assistant Professor with the Computer Architecture Department and Researcher with the Broadband Communications Group, Technical University of Catalunya, since 2005. In 2010, he joined the NaNoNetworking Center in Catalunya, where he is the Scientific Director. He is an Editor of Nano Communication Networks and founder of the ACM NANOCOM conference, the IEEE MONACOM workshop, and the N3Summit. He has also founded the LISPmob open-source initiative along with Cisco. He has been a Visiting Researcher with Cisco Systems, San Jose, CA, USA, and Agilent Technologies, Santa Clara, CA, USA, and a Visiting Professor with the Royal Institute of Technology (KTH), Stockholm, Sweden, and the Massachusetts Institute of Technology (MIT), Cambridge, MA, USA. He has given more than 10 invited talks (MIT, Cisco, INTEL, MIET, Northeastern University, etc.) and coauthored more than 15 journal and 40 conference papers. His main research interests are future architectures for the Internet and nanoscale communications.